Modelling and evaluating a solar pyrolysis system

Sánchez, M, Nixon, J & Clifford, B

Original citation & hyperlink:
Sánchez, M, Nixon, J & Clifford, B 2018, 'Modelling and evaluating a solar pyrolysis system' *Renewable Energy*, vol 116, pp. 630-638
https://dx.doi.org/10.1016/j.renene.2017.10.023

DOI 10.1016/j.renene.2017.10.023
ISSN 0960-1481
ESSN 1879-0682

Publisher: Elsevier

Modelling and evaluating a solar pyrolysis system

M. Sánchez[a], B. Clifford[a] and J. D. Nixon[b]*

[a] Kingston University, Faculty of Science, Engineering and Computing, Roehampton Vale campus, London, SW15 3DW, UK

[b] Coventry University, Faculty of Engineering, Environment and Computing, Coventry, CV1 2JH, UK

*corresponding author, E-mail: jonathan.nixon@coventry.ac.uk; Tel.: 024 7688 7688

Abstract

This study investigates the use of solar energy for producing biofuels through pyrolysis. A model is outlined to define the ideal parameters and evaluate the annual performance of a solar pyrolysis system. The model is demonstrated by considering a linear Fresnel reflector (LFR) system operating in Seville, Spain. The ideal operating temperature and total residence time were determined to be 571 K and 149 min, respectively. Subsequently, an LFR system was sized to have a total reactor length of 3.23 m, a polar inclination angle of 39° and an effective concentrating aperture area of 4.55 m^2. The maximum char yield fraction was found to be 40.8 wt.%; however, the annual variability of the solar input resulted in the system producing 1375 kg of biochar from 13.9 t of biomass. The model developed in this study can be applied to evaluate a range of solar thermal technologies in other localities for producing char, gar and oils through the pyrolysis process.

Keywords: linear Fresnel reflector (LFR); bioenergy; concentrating solar thermal power (CSP); slow pyrolysis; kinetics.

Nomenclature

A	Pre-exponential factor (1/s)
A_c	Effective concentrating aperture area (m^2)
A_s	Area of biomass particle (m^2)
b	Time constant (-)
B_i	Biot number (-)
C_p	Specific heat capacity of biomass (J/kgK)
DNI	Direct normal irradiance (W/m^2)
D_p	Biomass particle diameter (m)
D_r	Reactor diameter (m)
$E_{a,cj}$	Activation energy of char reaction (kJ/mol)
$E_{a,tj}$	Activation energy of tar reaction (kJ/mol)
F_{rp}	View factor between the reactor wall and the biomass particles (-)
h_p	Enthalpy for pyrolysis (MJ/kg)
h_r	Height of reactor from concentrating elements (m)
h_{rad}	Radiation heat transfer coefficient between reactor wall and biomass (W/m^2K)
$IAM_{(\theta t,\theta l)}$	Incidence angle modifier (-)
k_b	Thermal conductivity of biomass feedstock (W/mK)
k_{cj}	Char-reaction rate coefficient for each biomass component (1/s)
k_{tj}	Tar-reaction rate coefficient for each biomass component (1/s)
L_{op}	Reactor length for processing feedstock at an ideal operating temperature (m)
$L_{reactor}$	Total reactor length (m)
L_{heat}	Reactor length for biomass heating (m)
$\dot{m}_c$	Mass flow of produced char (kg/s)
$\dot{m}_g$	Mass flow of produced gas (kg/s)
$\dot{m}_j$	Mass flow of each component (kg/s)
$\dot{m}_{j0}$	Mass flow of each component introduced into the reactor (kg/s)
$\dot{m}_t$	Mass flow of produced tar (kg/s)
Q_{in}	Heat delivered to solar receiver absorbing surface (W)
Q_{loss}	Heat loss (W)
Q_u	Heat gained by biomass particles (W)
R	Universal gas constant (kJ/molK)
T_a	Ambient temperature (K)
T_i	Initial biomass temperature (K)
T_{op}	Ideal operating temperature (K)
t_{op}	Residence time (s)
t_{perm}	Total residence time (s)
T_r	Reactor wall temperature (K)
t_{heat}	Time for biomass particles to reach ideal operating temperature (s)
U_L	Heat loss coefficient (W/m^2K)
$\dot{V}$	Feeding rate (m^3/s)
V_s	Volume of each biomass particle (m^3)
X_{cj}	Char-gas mass proportions (-)
Y_c	Char yield fraction (%)
Y_j	Biomass component mass fraction (-)
α_s	Solar altitude angle (degrees)
γ_s	Azimuth angle from the south (degrees)
ε_p	Biomass void fraction (-)

ε_r	Inner reactor wall emissivity (-)
$\eta_{0=\theta}$	Collector optical efficiency at normal incidence angle (%)
$\eta_{end\text{-}loss}$	End-loss efficiency (%)
η_{total}	Total optical efficiency (%)
θ	Incidence angle (degrees)
θ_l	Longitudinal angle (degrees)
θ_p	Collector inclination angle (degrees)
θ_t	Transversal angle (degrees)
ρ_s	Biomass density (kg/m^3)

1. Introduction

Pyrolysis involves the thermal degradation of a substance in the absence of oxygen. The outputs from the process are gas and liquid products, and a carbon-rich solid residue called char. Densifying biomass into a biochar through pyrolysis provides several benefits as it increases energy density, reduces cost of transportation, makes it more grindable and provides a more homogeneous product. Whilst biochar can be utilised as a solid fuel, it can be used in a range of applications to achieve agricultural and environmental gains [1]. Biochar can be used for improving water retention and increasing soil fertility. Energy can be generated from pyrolysis gas and liquid products and, as biochar acts as a long-term carbon sink, there is the potential for systems to be carbon negative [2].

Slow pyrolysis, which involves relatively low temperatures (300-500 °C) and long residence times (minutes to hours), produces comparable liquid, gas and biochar yields. Fast pyrolysis (>500 °C) is used to increase the liquid fraction [3,4] and torrefaction (200-300 °C) is a mild form of pyrolysis used primarily for char production [5]. Typically, electricity or fossil fuels are used to provide the heat to a pyrolysis system, as the energy input can be easily controlled. However, to improve the sustainability of pyrolysis systems, alternative renewable energy sources are being investigated [6]. In hot rural areas there is an abundance of solar energy and grid electricity is often unavailable or unreliable, thus there has been a growing interest in the use of solar energy [7].

Concentrating solar thermal power (CSP) systems comprise a concentrator and a receiver. Several authors have investigated using a solar concentrator to provide the heat input to a receiver acting as a pyrolysis reactor. Morales et al. [8] evaluated the use of a parabolic trough collector (PTC) for pyrolysis using ray-tracing, but they did not go on to consider the impracticalities associated with solar tracking, off-axis rays and variable diurnal and seasonal irradiance levels. A fast pyrolysis system using a parabolic dish reflector (PDR) was proposed by Joardder et al. [9]. Their study focused on the biomass and solar resource availability in Bangladesh. Zeng et al. [10] outlined a two-stage heliostat-PDR concentrator with a shutter system for controlling heating rate and temperature of a pyrolysis reactor. Their study addressed the effects of temperature (600-2000 °C) and heating rate (5-450 °C/s) on char yield and properties, rather than on the performance of the system. Zeaiter et al. [11] built and tested a solar pyrolysis system using a Fresnel lens with two-axis tracking. The system reached temperatures of 550 °C and was used to pyrolyse waste rubber.

High temperature CSP systems have been examined for producing hydrogen and syngas. Abanades et al. [12] looked at obtaining hydrogen through the pyrolysis of natural gas using solar energy, and Kruesi et al. [13] studied solar gasification of bagasse. Z'Graggen & Steinfeld [14] investigated the use of a solar furnace for hydrogen production via steam-gasification, and they used a kinetic model to size the reactor and specify operational parameters. Several other authors have considered using a CSP system to provide heat indirectly for gasification processes [15-18]. Whilst an indirect system will increase cost and complexity, it does offer improvements in control and stability.

Issues with using a CSP system to provide the heat input to a pyrolysis reactor arise due to the variable nature of solar energy and the need for solar tracking. Additional difficulties are caused when using a PTC and PDR system, as they use expensive fragile receivers that need to move with the tracking system. An alternative CSP technology is the linear Fresnel reflector (LFR), which is a relatively simple and inexpensive technology. The receiver tower is fixed—removing the need for flexible hosing and a fragile evacuated tube—and insulates a single pipe or multiple tubes. Biomass could, therefore, be fed into this heated pipe and transformed into char, gas and pyrolysis oil products (see Figure 1).Unlike expensive parabolically shaped mirrors, the LFR also uses low-cost flat mirror element segments that can be rotated to control receiver temperature. However, an LFR's individual mirror elements are normally driven by independent motors, which can increase complexity. Another disadvantage of the LFR system is that it captures less energy than other solar collectors due to a lower optical efficiency. As with all CSP systems, there is a need for research to provide methods for sizing them for specific applications and evaluating daily and annual performance.

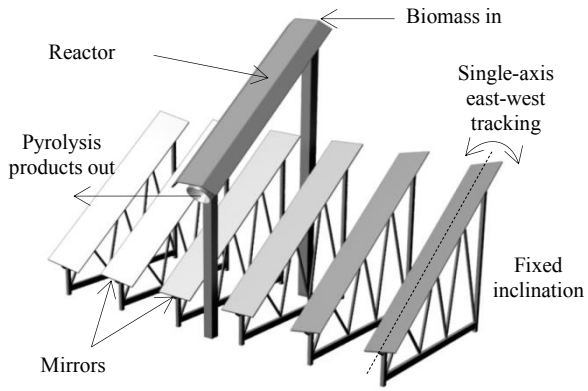

Figure 1: A linear Fresnel reflector with a polar alignment and east-west single-axis tracking.

This study aims to outline a theoretical model for sizing and evaluating the performance of solar pyrolysis systems by integrating pyrolysis kinetics, sun-earth geometry relations and solar thermal performance calculations. Using this model, the LFR technology and the impact of variable solar irradiance levels on biochar production and other system outputs is to be investigated. This will enable diurnal and seasonal changes in the product yields from a solar pyrolysis system to be modelled for specific locations.

In the following section, the method used to achieve this study's aim is outlined. In section 3, a model is developed for simulating solar pyrolysis reactions, and it is applied to a case study scenario in section 4. The paper concludes by evaluating the results and providing recommendations for future research on solar pyrolysis systems.

2. Method

In a solar pyrolysis reactor, biomass particles will increase in temperature from an initial biomass temperature, T_i, and then undergo pyrolysis at an ideal operating temperature, T_{op}. In kinetic studies, the pyrolysis products formed before a feedstock reaches a desired operating temperature are often neglected [2]. Therefore, two processes can be considered: (i) heating of biomass particles inside a reactor from an ambient temperature to an operating temperature, and (ii) pyrolysis reactions occurring at the operating temperature (see Figure 2).

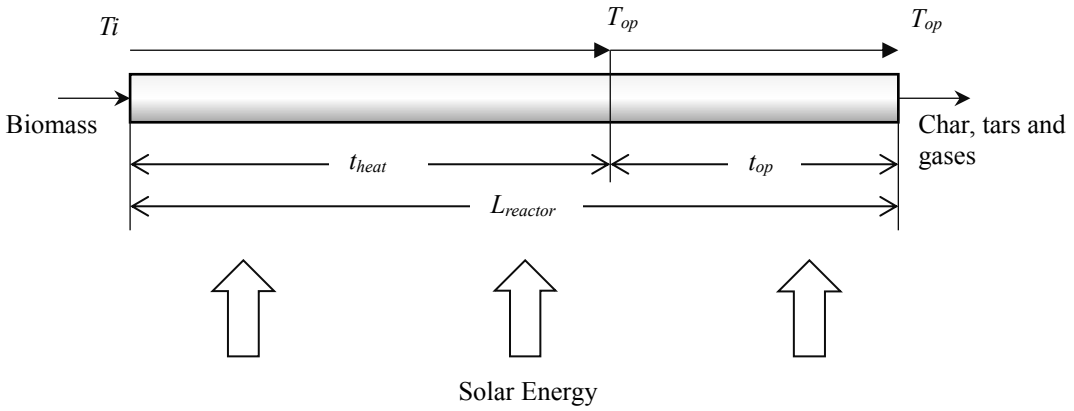

Figure 2: A solar pyrolysis reactor heating biomass particles from an inlet temperature to an ideal operating temperature.

The kinetic model adopted for this study is based on the works by Van der Weerdhof [19] and Miller and Bellan [20]. In this model, the individual cellulose, hemicellulose and lignin components, and their thermal decomposition into char, volatile tars and gases, are

222 considered. As cellulose, hemicellulose and lignin decompose at different rates and over
223 different temperature ranges [21], an ideal operating temperature, T_{op}, and residence time, t_{op},
224 for maximising char production can be determined. The total residence time is given by the
225 sum of a drying and heating residence time, t_{heat} (i.e. a period of time where biomass particles
226 are increasing in temperature) and a residence time, t_{op}, which is the length of time biomass is
227 processed at the operating temperature. In conventional reactors, the operating temperature
228 can be maintained; however, for a solar pyrolysis reactor, mean values have to be used to
229 calculate pyrolysis yields.
230
231 By simulating char production for varying operational temperatures and residence times, a
232 practical total length for the solar pyrolysis reactor, $L_{reactor}$, can be determined for a particular
233 feeding rate. The approach taken in this study is to simulate char production for increasing
234 temperatures and residence times until the yield increases by less than 10% in a one minute
235 period. At this point, the assumption is made that the ideal operating conditions have been
236 determined. The justification for this approach is that further increases in char production
237 rates would result in impracticalities associated with an excessive solar pyrolysis reactor
238 length.
239
240 The heat transferred to the biomass particles in the reactor is calculated by assuming a
241 lumped system approach outlined by Çengel [22]. A limitation of this approach is that it
242 assumes a uniform temperature inside the reactor. The heat transferred to the reactor from a
243 solar concentrator is determined using conventional CSP performance calculations [23].
244 Subsequently, the solar system can be sized to provide the required ideal operating
245 temperature at solar noon for a typical meteorological day. These specifications can be
246 achieved for different solar collectors and tracking arrangements.
247
248 To evaluate the annual performance of the sized solar pyrolysis system, it is assessed for a
249 typical meteorological year (TMY). Direct normal irradiance values are obtained from the
250 meteorological database, Meteonorm®. Thermal performance and incidence angle modifier
251 models for an LFR are presented based on previous studies by Nixon et al. [24-26].
252 MatLAB® is the software package used to run the simulations.
253

3. Model

The model outlined in this study is a generic model that could be adopted for any solar collector and is divided into three parts: modelling (i) the pyrolysis process to determine char, gas and tar yields, (ii) biomass particle heat transfer, and (iii) reactor heat gain and heat loss.

3.1 The pyrolysis process

Two different pyrolysis reactions are considered in the model: the char reaction, which produces char and gases, and the tar reaction, which produces volatile tars. Assuming that the pyrolysis of biomass follows first-order reaction kinetics, the mass flow of biochar produced, $\dot{m}_c$, can be estimated by integrating the following equation [19]:

$$\frac{\partial \dot{m}_c}{\partial t} = \sum_j k_{cj} X_{cj} \dot{m}_j \quad (1)$$

The index j represents the cellulose, hemicellulose and lignin biomass components, and k_{cj} is the char-reaction rate coefficient for each biomass component. X_{cj} represents the char-gas mass proportions that are produced during the char-reaction and $\dot{m}_j$ is the mass flow of each component at a particular moment.

$$\dot{m}_j = \dot{m}_{j0} e^{-(k_{cj}+k_{tj})t_{op}} \quad (2)$$

The char-reaction rate coefficients and tar-reaction rate coefficients, k_{tj}, can be calculated from the Arrhenius equation [27],

$$k_{cj} = A e^{-\frac{E_{a,cj}}{RT_{op}}} \quad (3)$$

$$k_{tj} = A e^{-\frac{E_{a,tj}}{RT_{op}}} \quad (4)$$

where A is a pre-exponential factor, E_a is the activation energy of the reaction, and R is the universal gas constant.

As the pyrolysis process takes place, the mass of each biomass component decreases and the mass of char formed increases. The mass flow of each component introduced into the reactor, $\dot{m}_{j0}$, depends on the feedstock characteristics and the biomass feedstock feeding rate, $\dot{V}$; it can be expressed as,

$$\dot{m}_{j0} = (1 - \varepsilon_p)\rho_s Y_j \dot{V} \quad (5)$$

The feedstock dependent parameters are the biomass void fraction, ε_p, density, ρ_s, and cellulose, hemicellulose and lignin mass fractions, Y_j.

The char yield fraction, Y_c, can now be calculated as,

$$Y_c = \frac{\dot{m}_c}{\sum_j \dot{m}_{j0}} \quad (6)$$

By integrating Eq.1, the mass flow of char, $\dot{m}_c$, and gas, $\dot{m}_g$, produced can be obtained as a function of the residence time, t_{op}, and k_{cj} and k_{tj}, which depend on the reactor temperature, T_{op}.

$$\dot{m}_c = \sum_j \left[\frac{k_{cj} X_{cj} \dot{m}_{j0}}{k_{cj} + k_{tj}} - \frac{k_{cj} X_{cj} \dot{m}_{j0}}{k_{cj} + k_{tj}} . e^{-(k_{cj}+k_{tj})t_{op}} \right] \quad (7)$$

$$\dot{m}_g = \sum_j \left[\frac{k_{cj} (1 - X_{cj}) \dot{m}_{j0}}{k_{cj} + k_{tj}} - \frac{k_{cj} (1 - X_{cj}) \dot{m}_{j0}}{k_{cj} + k_{tj}} . e^{-(k_{cj}+k_{tj})t_{op}} \right] \quad (8)$$

Similarly, the mass flow of produced tar, $\dot{m}_t$, can be calculated.

$$\dot{m}_t = \sum_j \left[\frac{k_{tj} \dot{m}_{j0}}{k_{cj} + k_{tj}} - \frac{k_{tj} \dot{m}_{j0}}{k_{cj} + k_{tj}} . e^{-(k_{cj}+k_{tj})t_{op}} \right] \quad (9)$$

By varying T_{op}, the mass flow of the pyrolysis products can be determined for different residence times. For each T_{op} value, a suitable residence time can be determined based on diminishing returns: i.e. a point where any additional pyrolysis product gains are not worth a further increase in residence time. A T_{op} value giving the highest mass flow of a particular pyrolysis component at the lowest t_{op} value can then be found in order to minimise reactor length. Having determined an ideal residence time and reactor temperature, the reactor length for processing biomass particles at the ideal operating temperature, L_{op}, can be specified for a particular reactor diameter, D_r.

$$L_{op} = \frac{4\dot{V} t_{op}}{\pi {D_r}^2} \quad (10)$$

3.2 Biomass particle heat transfer

A lumped system approach is used to describe the heating process that raises biomass particles in the reactor from an initial temperature to an ideal operating temperature. The approach is characterised by a Biot number, B_i, which depends on feedstock type and particle diameter, and the method is considered to be valid for Biot numbers of less than 0.1 [22].

$$B_i = \frac{h_{rad} V_s}{k_b A_s} \tag{11}$$

V_s is the volume of each biomass particle, A_s is the area of each particle and k_b is the thermal conductivity of the chosen biomass feedstock.

The radiation heat transfer coefficient between the reactor wall and the biomass particles, h_{rad}, can be calculated from,

$$h_{rad} = \frac{\sigma(T_i^2 + T_r^2)(T_i + T_r)}{\frac{1}{\varepsilon_r} - 1 + \frac{1}{F_{rp}}} \tag{12}$$

where σ is the Stefan-Boltzmann constant, T_r is the reactor wall temperature, ε_r is the inner reactor wall emissivity, and F_{rp} is the view factor between the reactor wall and the biomass particles. The time required for particles to reach an ideal operating temperature, t_{heat}, can be determined from,

$$t_{trans} = \frac{\ln\left(\frac{T_{op} - T_r}{T_i - T_r}\right)}{-b} \tag{13}$$

Parameter b is a time constant that is calculated from,

$$b = \frac{h_{rad} A_s}{\rho_s V_s C_p} \tag{14}$$

where C_p is the specific heat capacity of biomass.

The reactor length required for biomass heating, L_{heat}, can now be found:

$$L_{heat} = \frac{4\dot{V} t_{heat}}{\pi {D_r}^2} \tag{15}$$

The total reactor length, $L_{reactor}$, and total residence time, t_{perm}, are respectively calculated from $L_{heat} + L_{op}$ and $t_{heat} + t_{op}$.

3.3 Heat gain and loss

The heat gained by biomass particles, Q_u, in a reactor can be expressed by the following equation:

$$Q_u = h_{rad}\pi D_r L_{reactor}(T_r - T_i) \tag{16}$$

This assumes that the reactor is of uniform temperature, which, for solar systems, is only valid for low flow rates and short reactor lengths. If the temperature difference between the reactor wall and biomass particles is small, the heat gain found from Eq.(16) will be comparable to,

$$Q_u = \sum_j \dot{m}_{j0}\, C_p(T_{op} - T_i) \tag{17}$$

The required heat gain can be related to the enthalpy for pyrolysis, h_p, which defines the energy required to raise the feedstock from room temperature to reaction temperature, and convert the feedstock into pyrolysis products.

$$Q_u = \frac{h_p \rho_s (1 - \varepsilon_p)\frac{1}{4}\pi {D_r}^2 L_{reactor}}{t_{perm}} \tag{18}$$

The enthalpy for pyrolysis depends on reactor temperature due to changes in pyrolysis reaction chemistry, and enthalpy values stated in the literature have been calculated using different methods, feedstocks, reactor temperatures and assumptions regarding heat losses [28,29]. It is, therefore, difficult to use sensible and reaction enthalpies to determine an optimal operating temperature.

Assuming the reactor wall is of a uniform temperature, the heat loss, Q_{loss}, can be calculated from the ambient temperature, T_a, the solar-receiver geometry and a heat loss coefficient, U_L:

$$Q_{loss} = U_L \pi D_r L_{reactor}(T_r - T_a) \tag{19}$$

The heat loss coefficient is often expressed as a polynomial function of T_r.

$$U_L = a_2 T_r^2 - a_1 T_r + a_0 \tag{20}$$

Where an inert gas such as nitrogen is used for purging oxygen from the system, the heat transfer equations can be amended to include heating the gas and heat lost as the gas exits the system [28].

The energy delivered to a solar receiver's absorbing surface, Q_{in}, is given by,

$$Q_{in} = DNI.A_c.\eta_{(0=\theta)}.IAM_{(\theta_t,\theta_l)}.\eta_{end-loss} \quad (21)$$

where DNI is the direct normal irradiance, A_c is the effective concentrating aperture area of the collector, and $\eta_{0=\theta}$ is the optical efficiency of a collector when approaching rays are at a normal incidence angle, θ, to the aperture area. The optical efficiency includes properties such as transmittance, reflectance, absorbance and an intercept factor. These parameters depend on the sun's relative position to a solar system, so an Incidence Angle Modifier (IAM) is included to model daily and yearly changes in the optical efficiency. The IAM depends on the type of solar collector and tracking orientation being used, and it can be estimated from a product of the losses that occur due to off-axis rays in the transversal, θ_l, and longitudinal, θ_t, planes [26,30]. For a north-south alignment,

$$\theta_t = 90 - tan^{-1}\left(\frac{\tan\alpha_s}{\cos(90-\gamma_s)}\right) \quad (22)$$

$$\theta_l = 90 - \theta_p - \tan^{-1}\left(\frac{\tan\alpha_s}{\cos\gamma_s}\right) \quad (23)$$

where γ_s is the azimuth angle from the south, α_s is the solar altitude angle, and θ_p is the collector's inclination angle from the horizontal (e.g. when a polar-axis is used).

As the collector will be of a short length, additional end-losses, $\eta_{end\text{-}loss}$—which can be calculated from the height of the reactor from the concentrating elements, h_r—should be considered.

$$\eta_{end-loss} = 1 - \frac{h_r tan\theta_l}{L_{reactor}} \quad (24)$$

The total optical efficiency, η_{total}, at any given time is found from,

$$\eta_{total} = \eta_{(0=\theta)}.IAM_{(\theta_t,\theta_l)}.\eta_{end-loss} \quad (25)$$

The required effective concentrating aperture area to heat the reactor to a specific ideal operating temperature can now be determined for solar noon on a typical day of the year. This is achieved by assuming that the energy delivered to the solar reactor, Q_{in}, equals the sum of the heat gained by the biomass particles, Q_u, and the heat lost by the reactor, Q_{Loss}. With the solar pyrolysis system sized, the performance can be investigated by simultaneously solving T_r to determine daily varying reactor temperatures during a typically meteorological year.

4. Application to case study

The model is used to evaluate the annual performance of a solar pyrolysis system based on the linear Fresnel reflector technology. The chosen location is Seville, Spain, and ten-minute direct normal irradiance values have been taken for a TMY using the meteorological database Meteonorm®. The latitude angle for Seville is 37° and Figure 3 shows typical monthly irradiance and ambient temperature values.

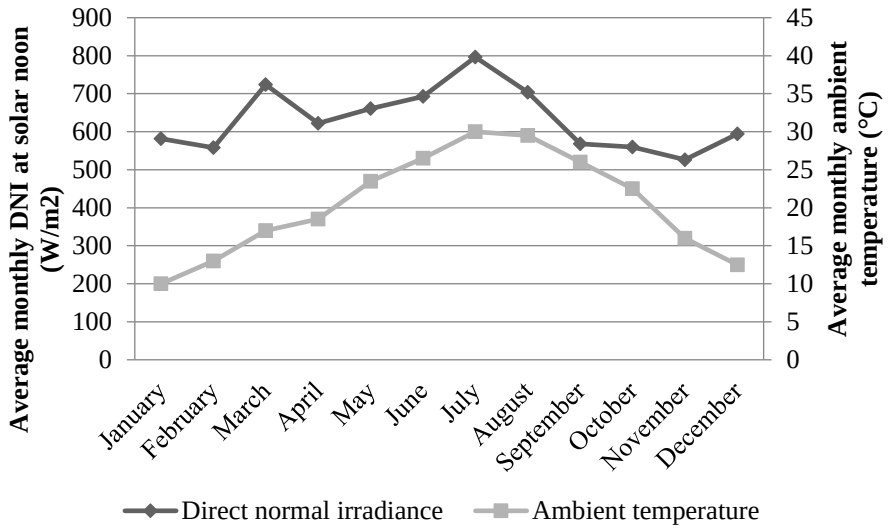

Figure 3: Average monthly direct normal irradiance values at solar noon and ambient temperatures in Seville, Spain.

For the LFR system, the collector's optical efficiency ($\eta_{0=\theta}$), reactor diameter and inner reactor wall emissivity are taken respectively as 75%, 70 mm and 0.18. In order to mitigate the effect of collector end-losses, the tracking orientation considered is a polar-axis with east-west tracking. The maximum reduction in annual end-losses is achieved by an inclination angle, θ_p, of 39º. For the purposes of this study, a uniform reactor wall temperature distribution is assumed and the difference between the reactor wall surface temperature and

388 the biomass particle temperature is taken as 10 ºC. Differences in reactor wall and particle
389 temperature have been evaluated in Ref. [31]. The reactor is assumed to process biomass in a
390 vacuum and therefore the heat transfer properties associated with a purging agent are not
391 considered.
392
393 The LFR's heat loss coefficient and $IAM_{(\theta l,\theta t)}$ are defined by,
394

$$U_L = 0.0000077.T_r^2 + 0.0042163.T_r + 0.5648278 \quad (26)$$

395

$$IAM_{\theta t} = 0.9967692 - 0.0024524\theta_t + 0.0000925\theta_t^2 - 0.0000021\theta_t^3 \quad (27)$$

396

$$IAM_{\theta l} = 1.0010489510 - 0.00505827510_l + 0.0000682110\theta_l^2 - 0.0000060431\theta_l^3 + 0.0000000504\theta_l^4 \quad (28)$$

397
398 where $IAM_{(\theta l,\theta t)}$ is obtained from the product of $IAM_{\theta t}$ and $IAM_{\theta l}$. The type of biomass to be
399 processed is wood chip, comprising of 46% cellulose, 32% hemicellulose and 22% lignin
400 mass fractions. The feeding rate for passing biomass through the solar pyrolysis reactor is set
401 at 0.005 m^3/h. The thermal conductivity, specific heat capacity and particle diameter of the
402 biomass feedstock are assumed to be 2273 J/kg.K [32], 0.1 W/m.K [31] and 0.01 m,
403 respectively. The model input parameters are summarised in Table 1 and the kinetic
404 parameters used for the pyrolysis of wood chip are shown in Table 2.

405 **Table 1:** Model input parameters.

Parameter	Units	Value
Feeding rate ($\dot{V}$)	m^3/s	0.005
Cellulose mass fraction ($Yj_{,cel}$)	-	0.46
Hemicellulose mass fraction ($Yj_{,hem}$)	-	0.32
Lignin mass fraction ($Yj_{,lig}$)	-	0.22
Biomass density (ρ_s)	kg/m^3	1250
Biomass void fraction (ε_p)	-	0.55
Specific heat capacity of biomass (C_p)	J/(kgK)	2273
Biomass particle diameter (D_p)	m	0.01
Inner reactor wall emissivity (ε_r)	-	0.18
View factor (F_{rp})	-	1
Thermal conductivity of biomass (k_b)	W/(mK)	0.1
Radiation heat transfer coefficient (h_{rad})	W/(m^2K)	3.825
Biot Number (Bi)	-	0.06375

406
407
408

Table 2: Kinetic parameters for the pyrolysis of wood chip.

Kinetic parameter	Units	Cellulose	Hemicellulose	Lignin
Char reaction				
Activation energy of reaction (E_a)	(kJ/mol)	150.5	145.7	67.77
Pre-exponential factor (A)	(s^{-1})	1.3e10	2.6e11	1.15e3
Char-gas mass properties (X_{cj})	-	0.35	0.6	0.75
Tar reaction				
Activation energy of reaction (E_a)	(kJ/mol)	196.5	202.4	100.8
Pre-exponential factor (A)	(s^{-1})	3.28e14	8.75e15	2.19e3

5. Results

5.1 Sizing the solar pyrolysis systems

The initial results obtained from the model relate to the ideal system parameters to increase char production during a typical meteorological day. For the chosen case study location, the ideal operating temperature, T_{op}, and total residence time, t_{perm}, were determined to be 571 K and 8939 s (149 min), respectively. The heating rate was approximately 4 K min^{-1}. For a biomass feeding rate of 5 l/h, the solar system required a total reactor length, $L_{reactor}$, of 3.23 m and an effective concentrating aperture area of 4.55 m^2. Daugaard and Brown [28] suggest that enthalpies for biomass pyrolysis will be in the region of 0.8 to 1.8 MJ/kg. A value of 0.7 MJ/kg has also been reported for wood chip being pyrolysed in a vacuum reactor [33]. Based on Eq.18, a temperature of 571 K would indicate an enthalpy of 1 MJ/kg, which correlates well with these findings.

The parameters of the sized system are summarised in Table 3.

Table 3: Sized solar pyrolysis system parameters.

Parameter	Value	Units
Effective concentrating aperture area (A_c)	4.55	m^2
Reactor diameter (D_r)	0.07	m
Collector inclination angle (θ_p)	39	°
Ideal temperature for pyrolysis (T_{op})	571	K
Reactor temperature (T_r)	581	K
Residence time (t_{op})	4800	s
Heating residence time (t_{heat})	4139	s
Total residence time (t_{perm})	8939	s
Permanent length of reactor (L_{op})	1.732	m
Heating length of reactor (L_{heat})	1.494	m
Total reactor length ($L_{reactor}$)	3.226	m
Height of reactor (h_r)	2.5	m

Figure 4 shows the performance of the system in terms of the conversion yields during a typical meteorological day in Seville, Spain. Potential pyrolysis product yields are compared for different operating temperatures achieved at specific times during the day. For the conditions achieved at solar noon, the maximum potential char yield obtained was found to be 40.8 wt.%; the gas and tar yields were 26.5 wt.% and 29.1 wt.%, respectively. These maximum yields cannot be obtained as the optimal conditions only occur at midday and the total residence time is 2.48 hrs. For the case study system, 49.5 kg of biomass can be fed into the system on a typical day, but only 6.4 kg of char would be obtained as the average daily char conversion yield would be 13 wt.%.

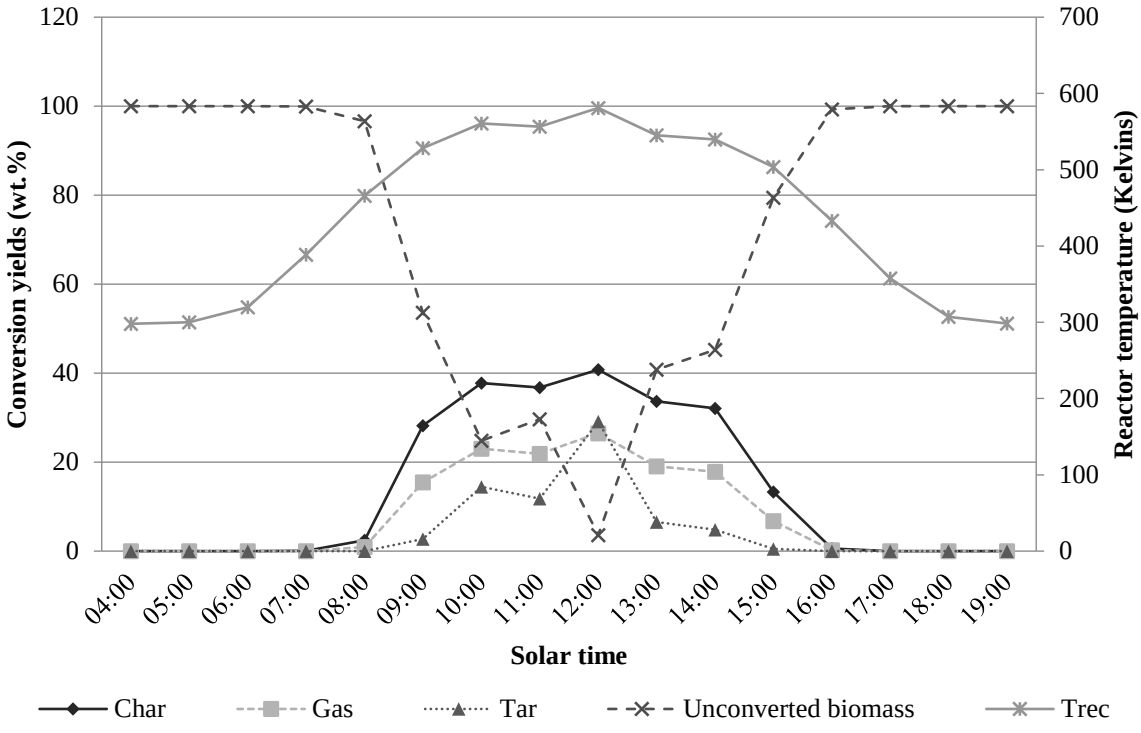

Figure 4: Char, gas and tar percentage yields of fed biomass for a typical day in Seville, Spain. The temperature of the solar reactor is shown on the secondary axis.

5.2 Evaluation of annual performance

The monthly quantities of char, gas and tar produced from the system are shown in Figure 5. Total char produced was found to be 1375 kg from 13.9 t of fed biomass, which is an average annual conversion of 10.1 wt.%. As the ideal char conversion efficiency was determined to be 40.8 wt.%, the annual variability of the solar input resulted in a 30 wt.% reduction in conversion efficiency. During July, the operational hours were at a maximum and the amount of biomass fed into the system was 1504 kg, which resulted in 133 kg of char being

produced. In March, 1241 kg was fed into the system and in August the input was 1315 kg. Even though a smaller amount of biomass was fed into the system during March and August, char yields were significantly higher at 191 kg and 170 kg, respectively.

The peak yields shown in Figure 5 for March and August are a result of the tracking orientation considered in this study. For a collector with a polar alignment and single-axis east-west tracking (see Figure 1), the incidence angle losses and end losses are lower when the sun is near the equinoxes. Therefore, even though the DNI is highest in July (see Figure 3) and more biomass can be fed into the system due to more operational daylight hours, the total yield of pyrolysis products is reduced. In the winter months, a low DNI and high incidence angle losses result in very small yields.

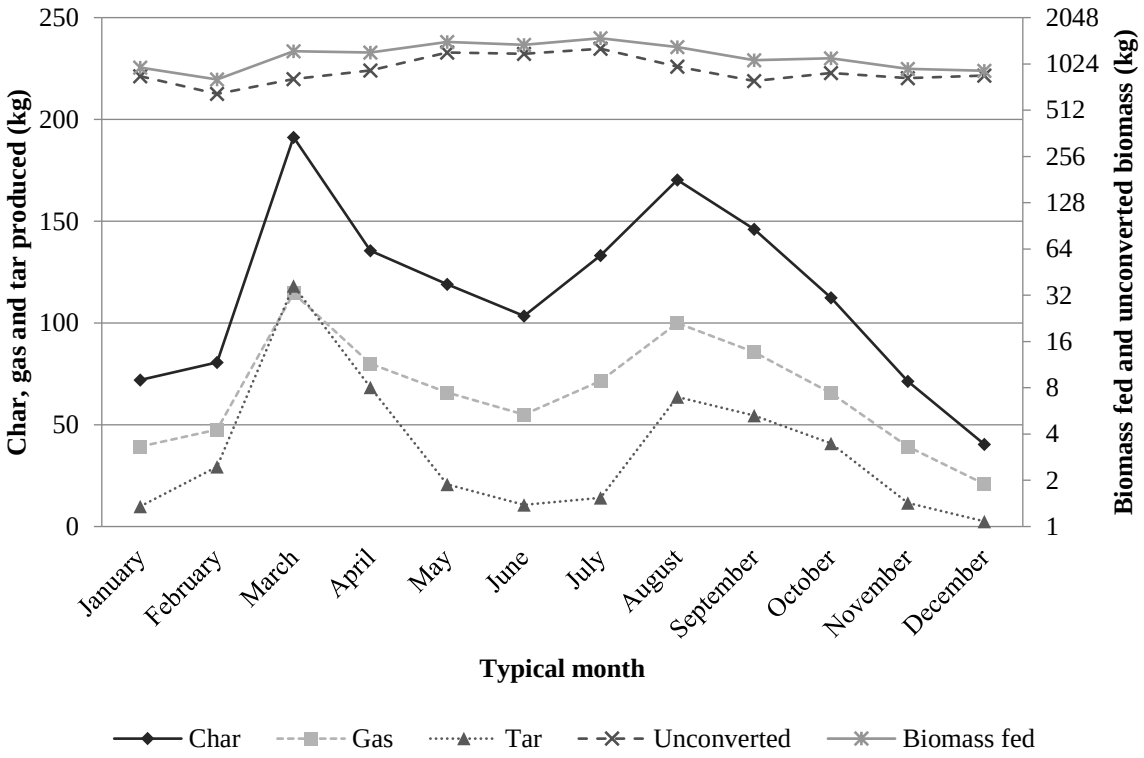

Figure 5: Char, gas and tar produced during a typical meteorological year in Seville, Spain. The secondary axis shows the amount of unconverted biomass and the amount of biomass fed into the system during these months.

To further examine the system's annual performance, Figure 6a-c shows the hourly char, gas and tar yields against reactor temperature for typical days in March, June and December. The system performance in March is comparable to a typical annual meteorological day (Figure 4) as the sun is near the equinox during this month and perpendicular to the effective

collector aperture area at solar noon. This results in a high total optical efficiency. Figure 6b shows that in June the char conversion at solar noon drops to 30 wt.% and yields drop rapidly either side of solar noon, as incident angle losses cause the reactor temperature to fall below 500 K. In December, DNI values at solar noon are still reasonably high at 600 W/m^2; however, the reactor temperature peaks at 500 K and quickly drops due to fewer daylight hours and high incidence angle losses. Consequently, char conversion yields reach only 12.9 wt.% at solar noon and the majority of the feedstock remains unconverted. The combined influence of end losses and longitudinal and transversal incident angle losses on the daily total optical efficiencies in March, June and December can be seen in Figure 7. In June, the total optical efficiency is 44% at solar noon, whereas the total optical efficiency in March remains significantly higher at 60%.

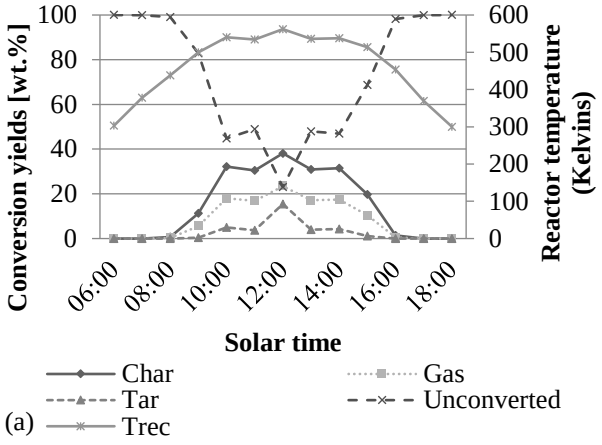

(a)

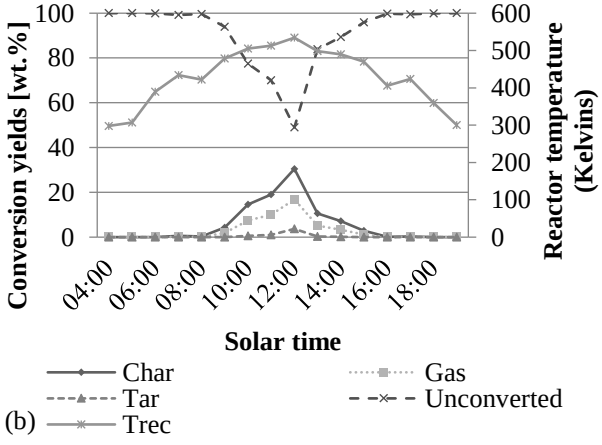

(b)

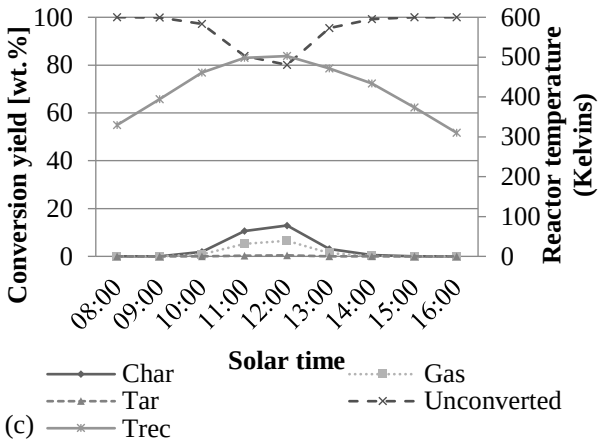

Figure 6a-c: Daily char, gas and tar yields for a solar pyrolysis reactor operating in Seville, Spain during a typical meteorological day in (a) March, (b) June and (c) December.

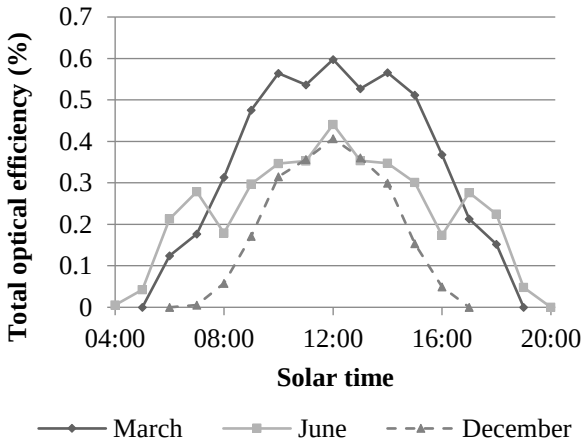

Figure 7: Total optical efficiency for the case study LFR system operating in Seville, Spain during a typical meteorological day in March, June and December.

6. Discussion

The peak char yield of 40.8 wt.% has a good agreement with yield values reported elsewhere for slow pyrolysis [2]. A total residence time of 149 min is a moderately high value for solar pyrolysis, and a reactor temperature of 581 K and a heating rate of 4 K min^{-1} are relatively low; however, these parameters are within the ranges reported in the literature [6]. The long residence time can be attributed to the low radiation heat transfer coefficient, which could be improved with a higher inner reactor wall emissivity. The high char, gas and tar yield fractions in the months of March and August are expected: incidence angle losses will be at a minimum near the equinoxes for solar collectors with a polar-axis tracking orientation. Therefore, even though DNI values are higher in summer months, the energy captured by the

solar system is reduced. The low values for winter months are due to reduced direct normal irradiance values and fewer daylight operating hours. Whilst the average annual char yield was only 10.1 wt.%, it is worth noting that annual conversion rates would be significantly improved if biomass was not fed into the system until a minimum specified reactor temperature were achieved; however, the total char produced would be reduced.

The financial implications of operating the system during periods of low irradiance would need to be assessed. The case study presented in this paper was based on the use of wood chips, which would need to be purchased, and low cost waste feedstocks would have different yield outputs. The sized solar system is relatively small at a length of 3.22 m and with an effective concentrating aperture area of 4.55 m^2. Thus, the system could be relatively cheap to construct. In hot rural developing areas—where electricity maybe unavailable and there is an abundance of agro-residues—1375 kg of biochar would be a valuable product for agricultural gains, and the other system outputs would be more usable for energy applications than raw waste feedstock.

The results presented in this study are highly dependent on the model assumptions, the tracking orientation considered and the type of solar collector. The model assumes a uniform temperature distribution and that pyrolysis reactions do not occur before biomass particles reach a specified ideal operating temperature. Whilst these are common assumptions in kinetic models for pyrolysis, it would be interesting to compare theoretical results with experimental findings. Furthermore, in a solar pyrolysis reactor, hot spots on the receiver would occur and biomass particles could exceed desired processing temperatures. A two-axis tracking arrangement would greatly improve pyrolysis products yields and reduce optical efficiency losses; however, it would involve a moving reactor and significantly increase complexity.

As with all pyrolysis reactors, additional equipment would be needed to separate out the different products. Pyrolysis oils and non-condensable gases can be separated in a condenser with further clean-up operations performed depending on the intended downstream application. Separating the char and unconverted biomass could be difficult and it would involve the use of gravity separators. Although this could add expense and complexity to the system, the model could be amended to consider unconverted feedstock being recycled and fed back into the system. This would improve system performance during periods of low

solar energy input. Alternatively, the entire solid yield could be fed back into the system when char yields are significantly low or a fraction of the mixture could be combusted to provide an additional heat input. Another extension to the model would be to consider higher feeding rates and controlling the feed rate to maintain a more constant reactor temperature. In further work, the techno-economic feasibility of different system configurations could also be investigated. Rather than designing a solar pyrolysis system for a typical meteorological day, different parameters could be used. For example, the system could be oversized using a concept such as the solar multiple and different tracking orientations could be compared. The benefit of the model outlined in this study is that it can be easily adopted by other researchers to investigate and compare different CSP technologies, system configurations and localities.

7. Conclusion

A model for sizing and evaluating solar pyrolysis systems has been outlined and applied to a configuration comprising a linear Fresnel reflector with a polar axis east-west tracking orientation. At solar noon, on a typical metrological day in Seville, Spain, a maximum char yield of 40.8 wt.% was obtained. The influence of variable irradiance levels resulted in an annual average char yield of 10.1 wt.%. We consider the LFR system to be a promising option for producing biochar, as it has many benefits as a solar pyrolysis reactor in comparison to more conventional concentrating solar thermal systems.

Figures and tables

Figure 1: A linear Fresnel reflector with a polar-axis tracking orientation.

Figure 2: A solar pyrolysis reactor heating biomass from an inlet temperature to an ideal operating temperature.

Figure 3: Average monthly direct normal irradiance values at solar noon and ambient temperatures in Seville, Spain.

Figure 4: Char, gas and tars percentage yields of fed biomass for a typical day in Seville, Spain. The temperature of the solar reactor is shown on a secondary axis.

Figure 5: Char, gas and tars produced for a typical meteorological year. The secondary axis shows the amount of unconverted biomass and the amount of biomass fed into the system during these months.

Figure 6a-c: Daily char, gas and tar yields for a solar pyrolysis reactor operating in Seville, Spain during a typical meteorological day in (a) March, (b) June and (c) December.

Figure 7: Total optical efficiency for the case study LFR system operating in Seville, Spain during a typical meteorological day in March, June and December.

Table 1: Model input parameters.

Table 2: Kinetic parameters of wood chip.

Table 3: Sized solar pyrolysis system parameters.

References

[1] Manyà JJ. Pyrolysis for biochar purposes: a review to establish current knowledge gaps and research needs. Environ Sci Technol 2012;46:7939-54.

[2] Hornung A. Transformation of Biomass: Theory to Practice. : John Wiley & Sons, 2014.

[3] Bruun EW, Ambus P, Egsgaard H, Hauggaard-Nielsen H. Effects of slow and fast pyrolysis biochar on soil C and N turnover dynamics. Soil Biol Biochem 2012;46:73-9.

[4] Duman G, Okutucu C, Ucar S, Stahl R, Yanik J. The slow and fast pyrolysis of cherry seed. Bioresour Technol 2011;102:1869-78.

[5] Batidzirai B, Mignot APR, Schakel WB, Junginger HM, Faaij APC. Biomass torrefaction technology: Techno-economic status and future prospects. Energy 2013;62:196-214.

[6] Goyal HB, Seal D, Saxena RC. Bio-fuels from thermochemical conversion of renewable resources: A review. Renewable and Sustainable Energy Reviews 2008;12:504-17.

[7] Panwar NL, Kaushik SC, Kothari S. Role of renewable energy sources in environmental protection: A review. Renewable and Sustainable Energy Reviews 2011;15:1513-24.

[8] Morales S, Miranda R, Bustos D, Cazares T, Tran H. Solar biomass pyrolysis for the production of bio-fuels and chemical commodities. J Anal Appl Pyrolysis 2014;109:65-78.

[9] Joardder MH, Halder PK, Rahim A, Paul N. Solar Assisted Fast Pyrolysis: A Novel Approach of Renewable Energy Production. Journal of Engineering 2014.

[10] Zeng K, Minh DP, Gauthier D, Weiss-Hortala E, Nzihou A, Flamant G. The effect of temperature and heating rate on char properties obtained from solar pyrolysis of beech wood. Bioresour Technol 2015;182:114-9.

[11] Zeaiter J, Ahmad MN, Rooney D, Samneh B, Shammas E. Design of an automated solar concentrator for the pyrolysis of scrap rubber. Energy Conversion and Management 2015;101:118-25.

[12] Abanades S, Tescari S, Rodat S, Flamant G. Natural gas pyrolysis in double-walled reactor tubes using thermal plasma or concentrated solar radiation as external heating source. Journal of natural gas chemistry 2009;18:1-8.

[13] Kruesi M, Jovanovic ZR, Steinfeld A. A two-zone solar-driven gasifier concept: Reactor design and experimental evaluation with bagasse particles. Fuel 2014;117:680-7.

606 [14] Z'Graggen A, Steinfeld A. Hydrogen production by steam-gasification of carbonaceous
607 materials using concentrated solar energy–V. Reactor modeling, optimization, and scale-up.
608 Int J Hydrogen Energy 2008;33:5484-92.

609 [15] Ravaghi-Ardebili Z, Manenti F, Corbetta M, Pirola C, Ranzi E. Biomass gasification
610 using low-temperature solar-driven steam supply. Renewable Energy 2015;74:671-80.

611 [16] Hathaway BJ, Honda M, Kittelson DB, Davidson JH. Steam gasification of plant
612 biomass using molten carbonate salts. Energy 2013;49:211-7.

613 [17] Nickerson TA, Hathaway BJ, Smith TM, Davidson JH. Economic assessment of solar
614 and conventional biomass gasification technologies: Financial and policy implications under
615 feedstock and product gas price uncertainty. Biomass Bioenergy 2015;74:47-57.

616 [18] Tanaka Y, Mesfun S, Umeki K, Toffolo A, Tamaura Y, Yoshikawa K. Thermodynamic
617 performance of a hybrid power generation system using biomass gasification and
618 concentrated solar thermal processes. Appl Energy 2015;160:664-72.

619 [19] Van der Weerdhof MW. Modelling the pyrolysis process of biomass particles. 2010.

620 [20] Miller R, Bellan J. A generalized biomass pyrolysis model based on superimposed
621 cellulose, hemicelluloseand liqnin kinetics. Combustion Sci Technol 1997;126:97-137.

622 [21] Jahirul MI, Rasul MG, Chowdhury AA, Ashwath N. Biofuels production through
623 biomass pyrolysis—a technological review. Energies 2012;5:4952-5001.

624 [22] Cengel YA, Hernán Pérez J. Heat transfer: a practical approach. Transferencia de calor/.
625 2004.

626 [23] Duffie JA, Beckman WA. Solar engineering of thermal processes. 3rd ed. New York:
627 John Wiley & Sons, 2006.

628 [24] Nixon JD, Dey PK, Davies PA. Design of a novel solar thermal collector using a multi-
629 criteria decision-making methodology. J Clean Prod 2013;59:150-9.

630 [25] Nixon J, Davies P. Construction and Experimental Study of an Elevation Linear Fresnel
631 Reflector. Journal of Solar Energy Engineering 2016;138:031001.

632 [26] Nixon JD, Davies PA. Cost-exergy optimisation of linear Fresnel reflectors. Solar
633 Energy 2012;86:147-56.

634 [27] Luo Z, Wang S, Cen K. A model of wood flash pyrolysis in fluidized bed reactor.
635 Renewable Energy 2005;30:377-92.

636 [28] Daugaard DE, Brown RC. Enthalpy for pyrolysis for several types of biomass. Energy
637 Fuels 2003;17:934-9.

638 [29] Atsonios K, Panopoulos KD, Bridgwater AV, Kakaras E. Biomass fast pyrolysis energy
639 balance of a 1kg/h test rig. International Journal of Thermodynamics 2015;18:267-75.

640 [30] Morin G, Dersch J, Platzer W, Eck M, Häberle A. Comparison of Linear Fresnel and
641 Parabolic Trough Collector power plants. Solar Energy 2012;86:1-12.

642 [31] Ellens CJ. Design, optimization and evaluation of a free-fall biomass fast pyrolysis
643 reactor and its products. 2009.

644 [32] Shackley S, Hammond J, Gaunt J, Ibarrola R. The feasibility and costs of biochar
645 deployment in the UK. Carbon Management 2011;2:335-56.

646 [33] Roy C, Lemieux R, de Caumia B, Blanchette D. Processing of wood chips in a
647 semicontinuous multiple-hearth vacuum-pyrolysis reactor. In: Anonymous : ACS
648 Publications; 1988.

649